





Article

Looking for a Safe Bridge: Synthesis of P3HT-Bridge-TBO Block-Copolymers and Their Performance in Perovskite Solar Cells

Aleksandra N. Zhivchikova ^{1,2} , Irina V. Klimovich ³, Maxim E. Sideltsev ¹, Aly Elakshar ² , Artur T. Kapasharov ¹, Alexander V. Akkuratov ¹ , Albert G. Nasibulin ², Keith J. Stevenson ⁴ and Marina M. Tepliakova ^{2,*} 

- ¹ Federal Research Center of Problems of Chemical Physics and Medicinal Chemistry of Russian Academy of Sciences, Academician Semenov Avenue 1, 142432 Chernogolovka, Russia
² Skolkovo Institute of Science and Technology, Bolshoy Boulevard 30, bld. 1, 121205 Moscow, Russia
³ ChemRAR, 2a-1, Rabochaya St. Khimki, 141401 Moscow, Russia
⁴ Department of Chemistry, Moscow State University, 1 Leninskiye Gory, 119991 Moscow, Russia
* Correspondence: marina.tepliakova@skoltech.ru

Abstract: Here, we present a synthesis of three novel conjugated block-copolymers (BCP) with general formula P3HT-bridge-TBO, where P3HT is a poly(3-hexyl)thiophene, TBO is a thiophene-benzothiadiazole block, and the bridge is composed of two fluorene units (FF) or two thiophenes (TT) or a mixture (TF). It is demonstrated that the physicochemical properties of the materials with different bridges are similar. Furthermore, P3HT-bridge-TBO materials are investigated in PSCs with classical n-i-p configuration for the first time. PSCs with BCPs reach average efficiencies with a top of 14.4% for P3HT-FF-TBO. At the same time, devices demonstrate spectacular long-term operation stability after 1000 h under constant illumination with minor changes in efficiency, while PSCs with state-of-the-art hole-transport layer demonstrate unstable behavior. This groundbreaking work demonstrates the potential of BCP to ensure the stable operation of perovskite photovoltaics.

Keywords: block-copolymers; double hole-transport layers; perovskite solar cells



Citation: Zhivchikova, A.N.; Klimovich, I.V.; Sideltsev, M.E.; Elakshar, A.; Kapasharov, A.T.; Akkuratov, A.V.; Nasibulin, A.G.; Stevenson, K.J.; Tepliakova, M.M. Looking for a Safe Bridge: Synthesis of P3HT-Bridge-TBO Block-Copolymers and Their Performance in Perovskite Solar Cells. *Organics* **2023**, *4*, 97–108. <https://doi.org/10.3390/org4010008>

Academic Editors: Wim Dehaen, Michal Szostak and Huaping Xu

Received: 31 December 2022

Revised: 14 February 2023

Accepted: 23 February 2023

Published: 27 February 2023



Copyright: © 2023 by the authors. Licensee MDPI, Basel, Switzerland. This article is an open access article distributed under the terms and conditions of the Creative Commons Attribution (CC BY) license (<https://creativecommons.org/licenses/by/4.0/>).

1. Introduction

Conjugated polymers consisting of alternating donor and acceptor units are attractive semiconducting materials with applications spanning all fields of organic electronics [1–4]. Such a popularity of these materials grew out of the straightforward tunability of electronic structure, charge transfer and film formation properties through the material design via incorporation of various donor and acceptor units. Additionally, the solubility of conjugated polymers in common organic solvents enables possible thin film deposition using printing and roll-to-roll techniques.

One of the possible directions toward the design of novel conjugated polymers is connecting independent donor and acceptor polymeric blocks through the bridge structure. Such block copolymers (BCPs) offer opportunities of obtaining a plethora of nanoscale-ordered structures due to self-assembling of materials in the bulk and in solutions [5,6]. The ability of BCPs to undergo nanoscale segregation and form stable conglomerates of donors and acceptors with the size of domains depending on the annealing regime was exploited in single-component organic solar cells [7].

The connection between two parts can be established by a simple C-C bond or have an individual structure [7]. In a recent work, it was shown that the nature of the connecting bridge may impact the photovoltaic performance of material [8]. In particular, a polymer containing a non-conjugated bridge demonstrated superior performance in organic solar cells, which was attributed to a more efficient charge separation due to hampering bimolecular charge recombination and, hence, a longer charge lifetime.

Poly(3-hexyl)thiophene (P3HT) is a very popular donor polymer in organic solar cell research and state-of-the-art polymeric hole-transport material for PSCs [9,10]. The widespread use of the material is mostly attributed to the simple synthesis and low price compared to other popular p-type semiconductors, such as PTAA. However, due to insufficient hole mobility, the material is usually applied in PSCs with doping, which increases the total price of device [11]. Nevertheless, P3HT is a great basis for the design of novel materials, and it can be particularly used as a donor part of block-copolymers.

Synthesis of fully conjugated polymer for organic electronic devices is usually conducted via cross-coupling reactions of functionalized P3HT with AB-type monomers, or with AA- and BB-type monomers, which is called modular strategy [12]. For example, a synthesis of BCP comprising benzodithiophene-bithiophene donor block and naphthalenediimide-selenophene acceptor lead to an efficient single-component organic solar cell [13].

Another photovoltaic technology, which attracts a lot of attention as a potential low-cost and highly efficient way to harvest solar energy is perovskite solar cells (PSCs). Possessing the efficiencies comparable to that of commercial crystal silicon solar cells, perovskite material offers the opportunity for solution-based deposition and simple upscaling using printing techniques [14,15]. The main challenge hampering PSC commercialization is the low stability of devices. Among the factors leading to stability decrease, there are phase instability under working conditions, thermal-, photo- and electrochemical degradation, reaction with moisture and oxygen of the air, etc. [16–18]. One of the well-studied components of the perovskite degradation mechanism is the reversible decomposition of the photoactive layer and migration of volatile decomposition products from the structure, which yet may be suppressed by using appropriate hole-transport layers with all the features for efficient charge transfer and good encapsulation properties [19,20].

Recent research has revealed the exceptional potential of a double hole-transport layer based on a combination of organic and inorganic p-type materials to efficiently conserve perovskite material and provide selective hole extraction [13]. However, it was shown that the organic component polytriarylamine (PTAA) requires further optimization [21,22].

The unique film-formation properties of BCPs owed to their ordering in thin films ensure improved charge transfer properties, which makes these materials promising for application as charge-transport layers in perovskite solar cells. The number of such reports is limited to the work of Ma et al., where three BCPs containing P3HT block and the second block incorporating either silolodithiophene or cyclopentadithiophene or dithienopyrrole were investigated as hole-transport layer in inverted p-i-n perovskite solar cells [23]. The special interlayer based on poly(sulfobetaine methacrylate) zwitterionic polymer was used atop BCPs to improve affinity of the surface to DMF and, hence, refine the quality of perovskite film. The superior characteristics of devices with silolodithiophene-based BCPs were attributed to proper material's energy level alignment with that of perovskite, and efficient hole-extraction.

Another example of the rational design of a block copolymer demonstrates a random copolymer RCP based on benzodithiophene and 2,1,3-benzothiadiazole [24]. The material was engineered to provide perfect energy level alignment (HOMO = -5.41 eV) and high charge transfer properties (hole mobility up to $1.85 \times 10^{-3} \text{ cm}^2 \text{ V}^{-1} \text{ s}^{-1}$). Application of RCP as dopant-free HTM in classical PSCs enabled high efficiency PCE = 17.3%.

In this work, we designed and synthesized a set of novel BCPs with the general structure of P3HT-bridge-TBO consisting of P3HT and thiophene-benzoxadiazole block using the modular strategy. The connection between blocks was established using thiophene-thiophene (TT) or thiophene-fluorene (TF), or fluorene-fluorene (FF) bridges, which is reflected in the names of materials. The undoped BCPs were applied as hole-transport materials in perovskite solar cells with n-i-p configuration. Moderate efficiencies of devices were achieved with 14.4% maximum for BCP with TT bridge, while the spectacular operational stability under constant illumination for more than 1000 h was observed for devices with all materials. The presented results reveal the potential of using block copolymers as

hole-transport materials for highly stable perovskite solar cells and pave a way for stable perovskite photovoltaics.

2. Materials and Methods

All solvents and reagents were purchased from Sigma-Aldrich (Darmstadt, Germany) or Acros Organics (Geel, Belgium), if not otherwise stated, and used as received or purified according to standard procedures.

Absorption spectra were obtained using an Avantes AvaSpec-2048 optical fiber spectrometer.

Molecular weight characteristics of conjugated polymers were obtained using a Shimadzu LC20 instrument. The measurements were performed using freshly distilled chlorobenzene as an eluent (flow rate 0.5 mL min^{-1} , column temperature 50°C). The column was calibrated using a series of custom-made F8BT standards with $\text{PDI} < 1.5$. Molecular weights of the F8BT standards were crosschecked additionally using a “Waters Alliance GPCV 2000” instrument equipped with a multi-angle scattering detector HELEOS II (Wyatt).

Purification of low molecular weight compounds (key building blocks) was performed using preparative GPC at Shimadzu LC20 instrument equipped with a Shodex GPC K-2001 50\AA $6 \mu\text{m}$, ($20 \times 300 \text{ mm}$). Freshly distilled toluene was used as an eluent (flow rate 1 mL min^{-1} , column temperature 40°C).

2.1. General Procedure Used for Synthesis of Block-Copolymers

Corresponding P3HT-bridge-Br (5 mol % or ca 0.01 eq), 4,7-Dibromo-5,6-bis(octyloxy) benzo[c][1,2,5]oxadiazole (1 eq), 2,5-Bis(trimethylstannyl)thiophene (1 eq), tetrakis (triphenylphosphine)palladium(0) (10 mol %), and 20 mL toluene were introduced into the 50 mL double-necked flask filled with argon, and refluxed for 24 h. Polymer formation was controlled during the reaction with gel permeation chromatography. At the end of the reaction the mixture was cooled to room temperature and 200 mL of deionized water was introduced. The organic fraction was extracted with toluene, washed three times with 150 mL of water. The solvent was partially removed at the rotary evaporator and polymeric fraction was precipitated with methanol. The precipitated product was filtered through cellulose thimble and purified using Soxhlet apparatus with acetone, hexane, dichloromethane, and chlorobenzene for 12 h each. The fraction extracted with chlorobenzene was precipitated with methanol and dried under reduced pressure during 24 h.

Polymer P3HT-TT-TBO was synthesized from P3HT-TT-Br. Yield = 64%. $M_w = 41 \text{ kDa}$, $\text{PDI} = 1.8$.

Polymer P3HT-TF-TBO was synthesized from P3HT-TF-Br. Yield = 39%. $M_w = 36 \text{ kDa}$, $\text{PDI} = 1.6$.

Polymer P3HT-FF-TBO was synthesized from P3HT-FF-Br. Yield = 26%. $M_w = 30 \text{ kDa}$, $\text{PDI} = 1.5$.

2.2. Device Fabrication

The ITO (Kintec, Kowloon, Hong Kong) was used as a bottom electrode. A combination of zinc and hydrochloric acid was used to create an electrode pattern on ITO. Samples were cleaned by sequential ultrasonication in isopropanol, water, and acetone, and then subjected to an air plasma treatment (50 W) for 5 min.

2.2.1. Deposition of Electron-Transport Layers

The 10% SnO_2 aqueous solution from AlfaAesar (Haverhill, MA, USA) was spin-coated at 4000 rpm in the air. The samples were annealed at 175°C for 20 min. The samples were then transferred to the glovebox and annealed at 150°C for 10 min. The layer of 6,6-phenyl-C61 butyric acid (PCBA) synthesized according to the literature [25] was spin-coated from solution in chlorobenzene (0.2 mg/mL) at 3000 rpm, and samples were annealed at 100°C for 10 min.

The ZnO solution was prepared by dissolving Zn acetate (100 mg) in monoethanolamine (33 μ L) and 2-methoxyethanol (1 mL) and spin-coated atop ITO at 6000 rpm. The samples were gradually heated from room temperature to 200 °C, where they were annealed for one hour. They were then heated to 300 °C and then returned to room temperature. ZnO was spin-coated with the CH₃NH₃I (MAI) solution (8 mg/mL in isopropanol) at 3000 rpm. The samples were annealed for 4 min at a temperature of 300 °C, then they were placed into the glovebox and heated for 5 min at 100 °C before the PCBA was deposited as described above.

2.2.2. Perovskite Deposition

CH₃NH₃PbI₃. To make the CH₃NH₃PbI₃ (MAPbI₃) perovskite solution (1.4 M), stoichiometric amounts of MAI and PbI₂ were dissolved in DMF and NMP (4:1). Perovskite ink was spin-coated onto the cooled substrates at 4000 rpm, quenched with toluene at 13 s and allowed to spin for 40 s. The samples were placed on the cold surface for 20 min, gradually heated to 80 °C, and then annealed for 5 min.

CsFAPbI₃. The CsFAPbI₃ solution with 1.4 M concentration was prepared by dissolving CsI (99 mg), (NH₂)₂CHI (434 mg), and PbI₂ (1474 mg) in DMF and DMSO (17:3). The perovskite layer was spin-coated at 4000 rpm, quenched with ethyl acetate after 17 s, and immediately placed onto the heater at 100 °C for 10 min annealing.

2.2.3. Deposition of Double-HTL and Top Electrodes

The referenced hot PTAA solution (6 mg/mL in chlorobenzene) was spin-coated on top of the perovskite at 3000 rpm. PTAA was synthesized as described in the literature [26].

Hot solutions of BCPs were deposited using preliminary optimized conditions (Figure S6).

The metal oxides were thermally evaporated from a tungsten boat under reduced pressure onto the whole surface of the sample. The source's power was gradually increased until a stable evaporation rate of 0.2 Å s^{−1} was reached. The thickness was controlled with quartz crystal.

The top electrodes (silver or aluminum) were thermally evaporated under reduced pressure via a shadow mask that defined the 0.072 cm² device area.

2.3. Device and Glass Characterization

The perovskite solar cells' characteristics were collected under a simulated AM1.5G illumination (100 mW/cm²), provided with a Newport Verasol AAA solar simulator and Advantest 6240 A source-measurement units. UV-vis spectra were measured in an inert atmosphere using an AvaSpec-2048-2UVVIS fiber spectrometer integrated with an MBraun glovebox. Electrochemical characterization was performed as reported previously [27].

3. Results and Discussion

In this work, three novel block copolymers with general structure P3HT-bridge-TBO were synthesized: where P3HT refers to a poly(3-hexyl)thiophene donor block, TBO is an acceptor block comprising thiophene (T) and benzoxadiazole (BO) moieties, and the bridge is a connector for donor and acceptor components. Three bridges were investigated as connections: TT, TF and FF, where F is fluorene. The synthetic pathway towards P3HT-bridge-TBO block copolymers is presented in Figure 1.

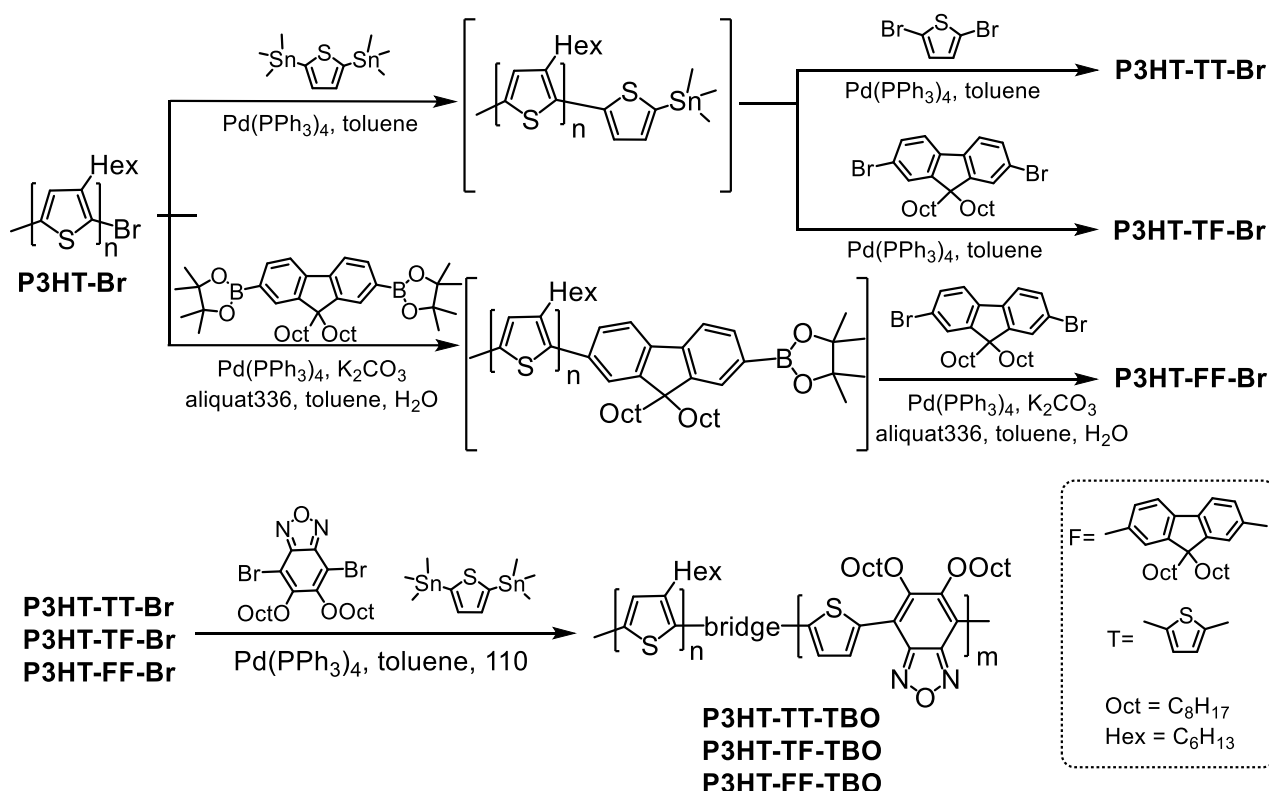


Figure 1. Synthesis of block copolymers by modular strategy.

The starting reagent for all materials was P3HT functionalized with Br synthesized using the Kumada reaction, as described previously (Scheme S1) [12]. This approach leads to the regioregular polymer with a low polydispersity index [28,29]. The structure of P3HT-Br was confirmed by ¹H NMR spectroscopy (Figure S1). The signals with a chemical shift of 2.62 ppm and 2.58 ppm correspond to methylene protons of hexyl groups on terminal thiophenes, respectively. The insignificant amount of unfunctionalized P3HT was discovered due to the difference of the integral intensity of signals, which is however considered potentially harmless to the final polymerization, as it bears no functional groups, which can terminate the reaction. Finally, the degree of polymerization was calculated based on the ratio between the intensity of signals of terminal thiophenes and that in the main chain. According to the calculation the molecular weight of the donor block was estimated to be 8.3 kDa, which was also confirmed by gel-permeation chromatography (Figure 2a).

At the next step, the bridging moiety was added to the donor part. The functionalized P3HT-Br was modified with a ten-fold excess of 2,5-bis(trimethylstannyl)thiophene and then with a ten-fold excess of 2,5-dibromothiophene under the condition of Stille cross-coupling to form P3HT-TT-Br. In order to form the P3HT-TF-Br at the second step Stille reaction with 2,7-dibromofluorene was used; and the building block with two fluorene units was obtained in two steps via Suzuki cross-coupling of P3HT-Br with a ten-fold excess of corresponding functionalized fluorene moieties (Figure 1). The modified P3HT-bridge-Br was purified and introduced into the polymerization reaction.

Synthesis of block-copolymers was conducted using a modular strategy previously reported for the synthesis of P3HT-b-DPP block-copolymer [12]. This synthetic strategy implies growing the second polymeric chain directly on the monofunctional P3HT-Br using AA and BB-type monomers. Such an approach is beneficial in terms of simple preparation of AA and BB-type monomers, possible energy level adjustment via monomer variation, and high purity of the target molecule.

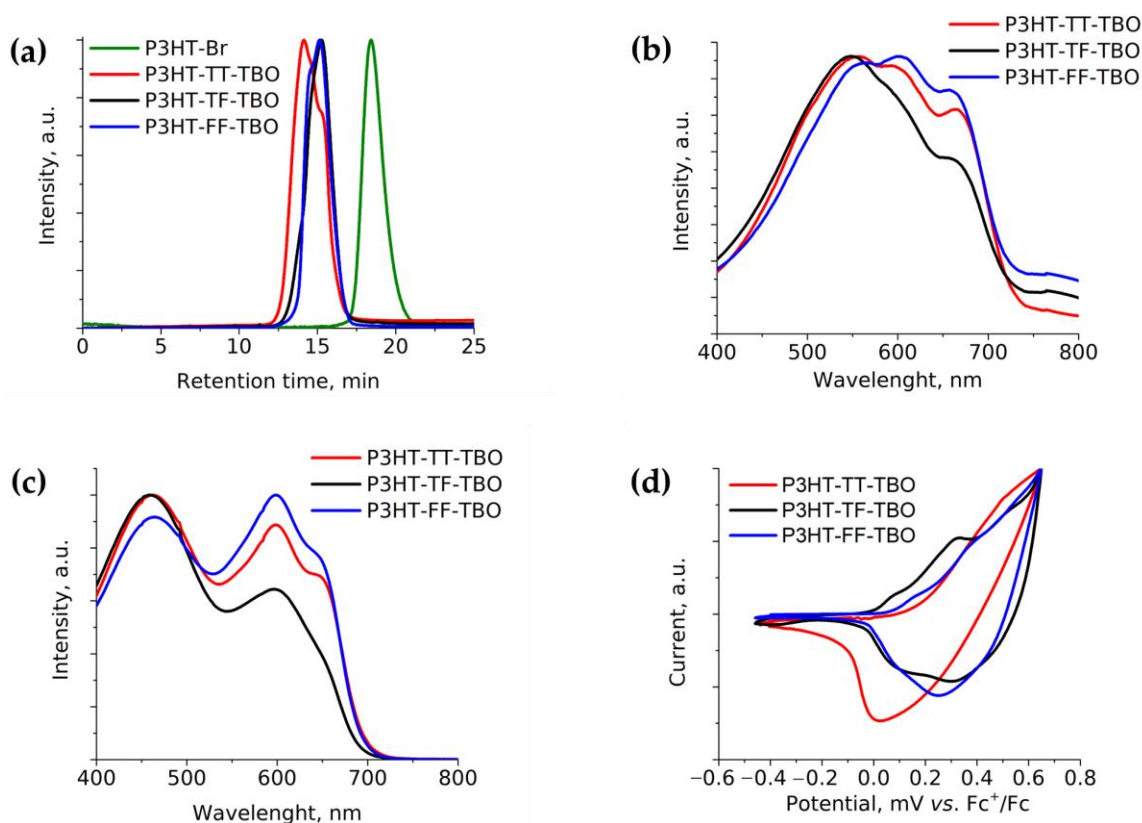


Figure 2. Gel permeation chromatography (a); absorption spectra in thin films (b) and in 1,2-dichlorobenzene solution (c) and cyclic voltammograms (d) of block copolymers.

Therefore, the P3HT-bridge-Br (0.01 eq.) basis was introduced into the Stille polycondensation with 2,5-Bis(trimethylstannyl)thiophene (1 eq.) and dibromosubstituted benzooxadiazole (1eq) in the presence of $Pd(PPh_3)_4$. After multistep purification from low molecular weight products, the successful synthesis of the polymer was evidenced with 1H NMR spectroscopy (Figures S2–S4) and gel permeation chromatography (Figure 2a). In particular, the signal of thiophene functionalized with bromine (chemical shift of 2.58 ppm) disappeared, while the signals corresponding to the fluorene bridge were observed at the 7.3–7.7 ppm range. The ratio between block components of each polymer is summarized in Table 1.

Table 1. Physicochemical, optical, and electrochemical properties of block-polymers P3HT-TT-TBO—P3HT-FF-TBO.

Name	M_w , kDa *	PDI *	P3HT:TBO Ratio **	λ_{edge}^{film} ABS, nm	E_g , eV	HOMO, eV	LUMO *, eV	T_d , °C
P3HT-TT-TBO	41	1.8	61:49	734	1.69	−4.92	−3.23	314
P3HT-TF-TBO	36	1.6	67:33	728	1.70	−4.94	−3.24	303
P3HT-FF-TBO	30	1.5	65:35	734	1.69	−4.91	−3.22	299

* M_w and PDI are extracted from GPC. ** block ratio is estimated from 1H NMR spectra.

The molecular weight (M_w) of P3HT-TT-TBO was found to be 41 kDa with a polydispersity index (PDI) of 1.8 and a ratio between P3HT and TBO of 61:49. BCPs with fluorene in the bridge moiety possessed lower molecular weights of 36 kDa and 30 kDa for TF and FF bridge, respectively, with the narrow molecular weight distribution (PDI = 1.6–1.5) and shorter length of TBO block.

The thermal stability of BCPs was studied by thermogravimetric analysis. According to the results, BCPs are thermally stable in the range of operating temperatures of perovskite

solar cells (Figure S9). Decomposition temperatures (T_d) of BCPs with TT, TF, and FF connection bridges were found to be 314, 303, and 299 °C, respectively, which is reflected in Table 1.

The electronic structures of the materials were evaluated using cyclic voltammetry and absorption spectroscopy in thin films (Figure 2b,d). In particular, the optical bandgap of polymers was determined as $E_g = 1240/\lambda_{\text{edge}}^{\text{film}} \text{ ABS}$, where the edge was found as a crossing between a tangent to the absorption maximum peak and the baseline. Polymers possess similar bandgaps in the range of 1.69–1.70 eV. Interestingly, a bathochromic shift of the peak corresponding to P3HT component was observed moving from the solution to the thin film, which suggests the ordering of the material in solid state. Furthermore, using cyclic voltammetry the highest occupied molecular orbital (HOMO) energy levels were calculated as $\text{HOMO} = -(E_{\text{ox}} + 4.8) \text{ eV}$, where E_{ox} is the onset of the oxidation peaks [21]. The onsets of oxidation potentials for P3HT-TT-TBO, P3HT-TF-TBO and P3HT-FF-TBO were found to be 0.12 V, 0.14 V, and 0.11 V corresponding to the HOMO energies of −4.92 eV, −4.94 eV, and −4.91 eV, respectively. For determination of the lowest unoccupied molecular orbital (LUMO) energy level the equation $\text{LUMO} = E_g + \text{HOMO}$ was used leading to −3.23, −3.24, and −3.22 eV LUMO levels of materials. Therefore, it is worth noting that the ratio of P3HT to TBO, as well as the structure of the connecting bridge, do not affect the energy of the boundary orbitals and the energy band gap (Table 1).

The estimated HOMO energy levels of the obtained BCPs were found in imperfect but suitable alignment with the valence band of the most popular perovskite material MAPbI_3 , which could lead to energy losses and lower characteristics of devices. Nevertheless, it was of particular interest to compare the performance of materials with various bridges in PSCs. Therefore, at the next step, the BCPs were investigated as hole-transport materials (HTLs) in PSCs and optimal deposition conditions for BCPs were identified. For this purpose, PSCs with classical n-i-p configuration were fabricated (Figure 3a). In brief, the bottom transparent electrode (ITO) was covered with SnO_2 electron-transport layer, which was further passivated with 6,6-phenyl- C_{61} butyric acid (PCBA) [25]. Furthermore, the photoactive layer $\text{CH}_3\text{NH}_3\text{PbI}_3$ (MAPbI_3) was spin-coated, and the hole-transport layer represented by one of the BCPs or polytriarylamine (PTAA) for the reference cells was deposited. In each optimization experiment, reference devices were fabricated with the PTAA synthesized using Suzuki polycondensation [26]. Finally, molybdenum oxide and silver electrodes were evaporated to complete the structure.

A total of 240 devices with block-copolymers and PTAA were fabricated to generate full and reliable statistics and define optimal deposition conditions (Figure S5). The distributions of power-conversion efficiencies (PCEs, %), open-circuit voltages (V_{OC} , mV), short-circuit current densities (J_{SC} , mA cm^{-2}), and fill factors (FF, %) for the devices with BCPs are summarized in Table 2. The values of the short-circuit current densities were confirmed using EQE (Figure S6).

Devices with BCPs delivered modest efficiencies with the highest PCE of 14.4% received for devices with P3HT-FF-TBO. The expected energy losses due to the mismatch between the energy levels of perovskite and polymers led to significantly lowered V_{OC} values compared to that of the reference devices.

Additionally, the noticeable hysteresis between forward and reverse scans was registered, which is usually related to the substantial density of defects on the interface between HTL and perovskite (Figure 3c). Taking into consideration the tendency of BCPs to self-assemble, we suggested as a reason for hysteresis behavior the formation of defects at the interface with perovskite functioning as sites for charge recombination [30].

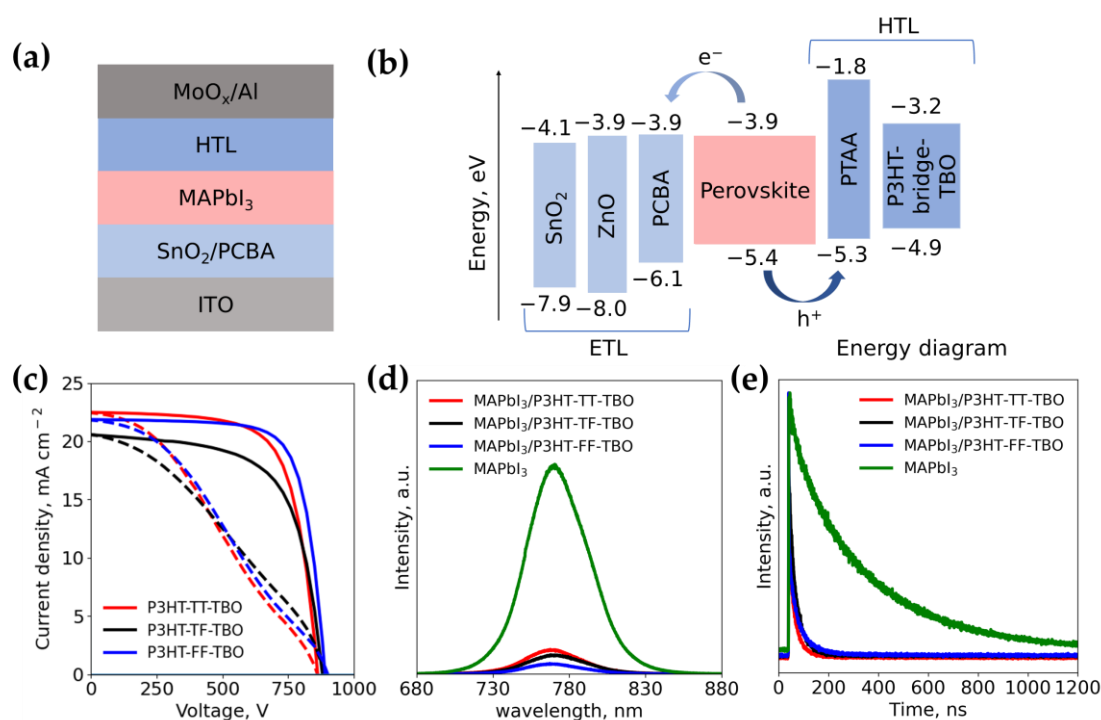


Figure 3. Device configuration used for BCP optimization experiments (a); energy diagram (b); J-V curves of PSCs fabricated under optimized conditions (the reverse scan is indicated as a dashed line, the forward scan is indicated as a solid line) (c); steady-state PL (d) and time-resolved PL (e) measurements of samples with configuration perovskite/HTL.

Table 2. Characteristics of perovskite solar cells with different BCPs presented as max (average \pm standard deviation).

Name	HI	V_{OC} , mV	J_{SC} , mA cm^{-2}	FF, %	PCE, %
MoO _x only	0.83	164 (260 \pm 70)	11.7 (7.3 \pm 3.1)	57 (35 \pm 13)	1.6 (0.6 \pm 0.7)
PTAA	0.07	1046 (1014 \pm 14)	22.2 (20.5 \pm 1.6)	76 (70 \pm 5)	17.3 (14.6 \pm 1.7)
P3HT-TT-TBO	0.36	861 (843 \pm 35)	22.5 (21.8 \pm 0.6)	70 (55 \pm 16)	13.4 (10.3 \pm 3.3)
P3HT-TF-TBO	0.30	895 (878 \pm 9)	20.8 (20.0 \pm 1.0)	64 (51 \pm 13)	11.6 (9.0 \pm 2.0)
P3HT-FF-TBO	0.37	835 (900 \pm 50)	23.4 (21.4 \pm 1.4)	73 (52 \pm 15)	14.4 (9.5 \pm 3.3)

The short lifetime of charges was confirmed by photoluminescence (PL) spectra of samples with configuration glass/MAPbI₃/HTL and glass/MAPbI₃ as reference. The efficient perovskite PL quenching and short lifetime of PL signal observed in time-resolved PL spectra of bilayer stacks with BCPs may be related to either their good hole-extracting ability or charge trapping on the defects. The PL decays were described with two exponential trends and fitted accordingly; the extracted carrier lifetimes are summarized in Table S1.

According to previous reports, the hysteresis issue was also observed in PSCs for devices with perovskite and BCP layers being in direct connection [23,24]. However, it was shown that an introduction of an additional zwitterionic interlayer allows the hysteresis to heal and push the characteristics of devices to higher levels [23].

As the hysteresis issue can be suppressed with the proper interlayer, we proceeded further with the investigation of the stability of PSCs with BCPs under various conditions.

Preliminary, the sensitivity of the photoactive layer to the moisture and oxygen of the air is a critical obstacle to practical application; therefore, the hydrophobicity of the perovskite coverage is crucial to ensure perovskite protection from harmful factors. For evaluating the hydrophobicity and quality of the coverage provided by BCPs we measured the contact angle (θ) of water with the surface of BCP films on the glass (Figure 4). The high values of contact angle $\theta = 94\text{--}97^\circ$ between water and BCP surface which did not change after 20 s indicated the hydrophobic nature of BCP films. Thus, we assume that the hydrophobic properties of block copolymers are sufficient to protect the photoactive layer from exposure to water.

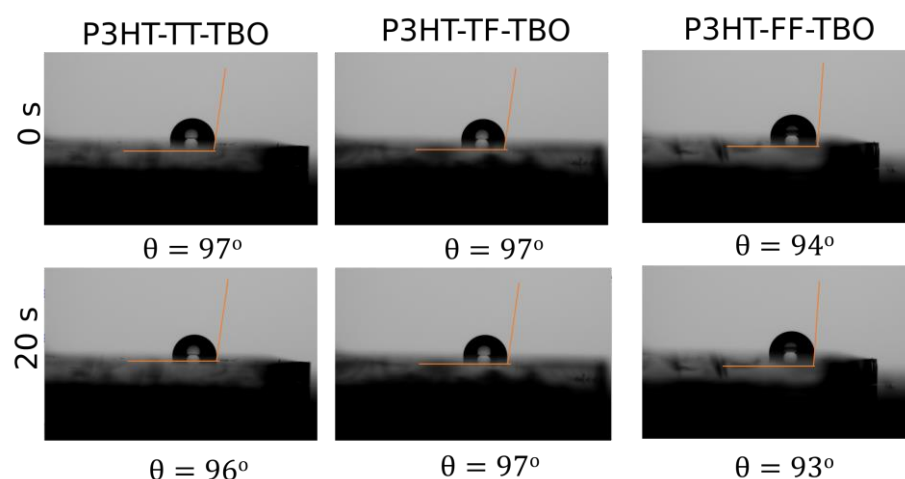


Figure 4. Contact angle of water on glass/BCPs samples.

Additionally, the surface of the glass/BCPs and glass/perovskite/BCPs samples was characterized using atomic force microscopy (AFM) (Figures S7 and S8). The surface of the sample with P3HT-TT-TBO is covered with high columnar-like formations, while the morphology of P3HT-TF-TBO and P3HT-FF-TBO is more uniform and reflects that of bare perovskite. Such an inhomogeneous surface of P3HT-TT-TBO may be related to the lower solubility of the polymer due to higher molecular weights.

At the next step, the stability of the devices under constant illumination was investigated (Figure 5). The previously reported modified architecture of PSCs using ZnO as ETL and CsFAPbI₃ perovskite was used in this experiment [21]. The lower ITO electrode was coated with a solution of ZnO and further passivated with MAI and PCBA. The photoactive layer was spin-coated and BCPs were deposited atop. The vanadium oxide and Al electrodes completed the architecture to be ITO/ZnO:MAI:PCBA/perovskite/BCPs/VO_x/Al [31].

The non-encapsulated devices were placed into a degradation chamber embedded in a glovebox with an inert atmosphere (oxygen and water concentration < 0.01 ppm). The illumination power of the white LEDs was $57 \pm 3 \text{ mW cm}^{-2}$ and the temperature was maintained within $45 \pm 1^\circ\text{C}$ for 1000 h, which corresponds to the degradation protocol ISOS-L-2I [32]. During the experiment, the current-voltage characteristics were monitored and the evolution of PCE for devices with BCPs and for PTAA are presented in Figure 5.

The low characteristics of fresh devices, which improve after some time under illumination, are common to this configuration and can be explained by a burn-in of defects. Devices containing P3HT-TT-TBO showed stable behavior with modest efficiencies during the whole experiment. PSCs with BCPs containing fluorene demonstrated an increase in efficiency since the starting point and stable work up to the end of the experiment. Current-voltage characteristics of degraded devices are given in Figure S10. It is interesting to note that for devices with P3HT-FF-TBO and P3HT-TF-TBO the hysteresis decreased significantly at the end of the experiment. Therefore, the probable reason for high hys-

teresis of fresh devices could be defective interface of the material with perovskite, which improved after exposure to light and temperature. Finally, the most unstable behavior was observed for the reference devices, which, however, stays in accordance with the previously reported results [21]. A decrease in the stability of devices with PTAA is related to the growth of polymer-based filamentous structures through the film of the photoactive layer. In sum, devices containing BCPs show excellent stability under constant illumination, the hysteresis was reduced for fluorene-containing materials, and devices with P3HT-TF-TBO demonstrated the best performance at the end of the stability test.

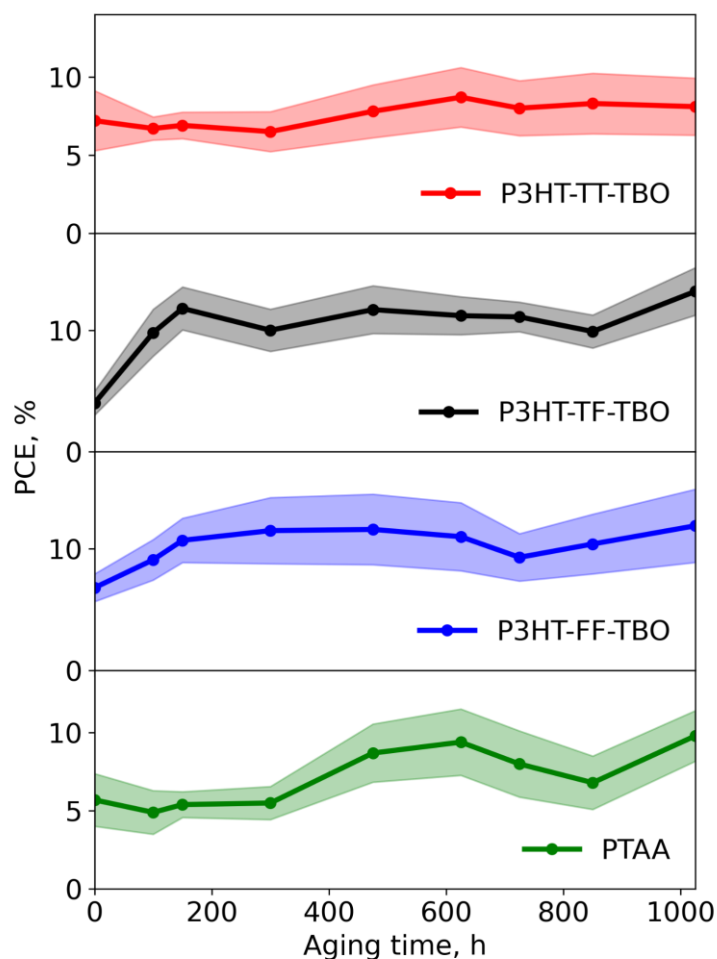


Figure 5. Evolution of efficiency of PSCs with BCPs and PTAA as organic components of hybrid HTL.

4. Conclusions

In this work, we designed and synthesized three conjugated block-copolymers with P3HT-bridge-TBO structure where the bridge structures are thiophene-thiophene, thiophene-fluorene, or fluorene-fluorene pairs. It was shown that the nature of the bridge does not significantly impact electronic structures of the materials and their morphology in thin films. However, the high molecular weight of P3HT-TT-TBO may lead to its reduced solubility in organic solvents and, thus, to the appearance of formations on the surface of thin films revealed by AFM.

Then, the materials were applied as organic components of hybrid HTL in n-i-p PSCs and demonstrated efficiencies up to 14.4% for P3HT-TT-TBO. The main losses of the efficiency were due to low values V_{OC} and hysteresis behavior. The possible strategy to enhance the efficiency could consist in introducing more donor units into the structure of individual polymeric blocks to lower HOMO level and avoid energy losses coming from energy level misalignment with perovskite valence band. Furthermore, using steady-state and time-resolved photoluminescence it was shown that PL intensity of perovskite covered

with all block copolymers is substantially quenched and charge carrier lifetime is short, which can be attributed to the good hole-extracting ability of presented block-copolymers.

Most importantly, devices with P3HT-bridge-TBO materials demonstrated high operation stability under constant illumination during 1000 h without a drop of characteristics, while fluorene-containing polymers P3HT-TF-TBO and P3HT-FF-TBO delivered even higher efficiencies at the end of the experiment without hysteresis.

The presented scientific findings reveal a great potential of block-copolymers as HTLs for highly stable PSCs.

Supplementary Materials: The following supporting information can be downloaded at: <https://www.mdpi.com/article/10.3390/org4010008/s1>, Scheme S1: Synthesis of P3HT-Br; Figure S1: Gel-permeation chromatography of P3HT-Br; Figures S2–S4: NMR Spectra; Figure S5: Optimization of deposition conditions; Figure S6: EQE; Figure S7: AFM of the samples with configuration perovskite/HTM; Figure S8: AFM of bare BCPs; Figure S9: TGA of block copolymers; Figure S10: J-V characteristics of degraded PSCs with P3HT-bridge-TBO block copolymers as HTM; Figure S11: Current-voltage characteristics for device with MoOx as HTL; Figure S12: Cross-sectional SEM of PSC; Table S1: Charge carrier lifetime extracted from time-resolved photoluminescence measurements.

Author Contributions: Conceptualization, I.V.K., A.N.Z. and M.M.T.; methodology, I.V.K. and M.M.T.; validation, I.V.K., A.N.Z. and M.M.T.; formal analysis, M.E.S., A.E. and A.T.K.; investigation, I.V.K., A.N.Z. and M.M.T.; resources, K.J.S. and A.G.N.; data curation, I.V.K., A.N.Z. and M.M.T.; writing—original draft preparation, A.N.Z., M.M.T. and A.V.A.; writing—review and editing, A.N.Z. and M.M.T.; visualization, A.N.Z.; supervision, M.M.T., A.V.A. and K.J.S.; project administration, K.J.S.; funding acquisition, K.J.S. All authors have read and agreed to the published version of the manuscript.

Funding: Microscopy studies were supported with the 1-NGP-1487 grant funded by Skolkovo foundation. Investigation of electronic properties of polymers was supported by the Ministry of Science and Higher Education of the Russian Federation within the project 122111700041-8 (FFSG-2022-0004).

Data Availability Statement: Not applicable.

Conflicts of Interest: The authors declare no conflict of interest.

References

1. Wang, X.; Sun, Q.; Gao, J.; Wang, J.; Xu, C.; Ma, X.; Zhang, F. Recent Progress of Organic Photovoltaics with Efficiency over 17%. *Energies* **2021**, *14*, 4200. [\[CrossRef\]](#)
2. Palani, P.; Subramanian, K. Conjugated polymer—A versatile platform for various Photophysical, Electrochemical and Biomedical applications: A Comprehensive review. *New J. Chem.* **2021**, *45*, 19182–19209. [\[CrossRef\]](#)
3. Kranthiraja, K.; Arivunithi, V.M.; Aryal, U.K.; Park, H.-Y.; Cho, W.; Kim, J.; Reddy, S.S.; Kim, H.-K.; Kang, I.-N.; Song, M.; et al. Efficient and hysteresis-less perovskite and organic solar cells by employing donor-acceptor type π -conjugated polymer. *Org. Electron.* **2019**, *72*, 18–24. [\[CrossRef\]](#)
4. Kranthiraja, K.; Park, S.H.; Kim, H.; Gunasekar, K.; Han, G.; Kim, B.J.; Kim, C.S.; Kim, S.; Lee, H.; Nishikubo, R.; et al. Accomplishment of Multifunctional π -Conjugated Polymers by Regulating the Degree of Side-Chain Fluorination for Efficient Dopant-Free Ambient-Stable Perovskite Solar Cells and Organic Solar Cells. *ACS Appl. Mater. Interfaces* **2017**, *9*, 36053–36060. [\[CrossRef\]](#)
5. Smith, K.; Lin, Y.-H.; Dement, D.; Strzalka, J.; Darling, S.; Pickel, D.; Verduzco, R. Synthesis and Crystallinity of Conjugated Block Copolymers Prepared by Click Chemistry. *Macromolecules* **2013**, *46*, 2636–2645. [\[CrossRef\]](#)
6. Orilall, M.C.; Wiesner, U. Block copolymer based composition and morphology control in nanostructured hybrid materials for energy conversion and storage: Solar cells, batteries, and fuel cells. *Chem. Soc. Rev.* **2011**, *40*, 520–535. [\[CrossRef\]](#)
7. Xiao, L.-L.; Zhou, X.; Yue, K.; Guo, Z.-H. Synthesis and Self-Assembly of Conjugated Block Copolymers. *Polymers* **2020**, *13*, 110. [\[CrossRef\]](#) [\[PubMed\]](#)
8. Lee, H.; Kim, D.; Cho, J.; Park, Y.; Kim, J.; Cho, K.; Lee, H.S.; Kim, D.H.; Cho, J.H.; Park, Y.D.; et al. Enhancement of interconnectivity in the channels of pentacene thin-film transistors and its effect on field-effect mobility. *Adv. Funct. Mater.* **2006**, *16*, 1859–1864. [\[CrossRef\]](#)
9. Jung, E.; Jeon, N.; Park, E.; Moon, C.; Shin, T.; Yang, T.-Y.; Noh, J.; Seo, J. Efficient, stable and scalable perovskite solar cells using poly(3-hexylthiophene). *Nature* **2019**, *567*, 511–515. [\[CrossRef\]](#) [\[PubMed\]](#)
10. Kleinschmidt, A.T.; Root, S.E.; Lipomi, D.J. Poly(3-hexylthiophene) (P3HT): Fruit fly or outlier in organic solar cell research? *J. Mater. Chem. A* **2017**, *5*, 11396–11400. [\[CrossRef\]](#)

11. Yaghoobi Nia, N.; Matteocci, F.; Cinà, L.; Di Carlo, A. High Efficiency Perovskite Solar Cell Based on Poly (3-hexylthiophene) (P3HT): The Influence of P3HT Molecular Weight and Mesoscopic Scaffold Layer. *ChemSusChem* **2017**, *10*, 3854–3860. [\[CrossRef\]](#)
12. Ku, S.-Y.; Brady, M.; Treat, N.; Cochran, J.; Robb, M.; Kramer, E.; Chabiny, M.; Hawker, C. A Modular Strategy for Fully Conjugated Donor-Acceptor Block Copolymers. *J. Am. Chem. Soc.* **2012**, *134*, 16040–16046. [\[CrossRef\]](#)
13. Park, C.G.; Park, S.H.; Kim, Y.; Nguyen, T.L.; Woo, H.Y.; Kang, H.; Yoon, H.J.; Park, S.; Cho, M.J.; Choi, D.H. Facile one-pot polymerization of a fully conjugated donor-acceptor block copolymer and its application in efficient single component polymer solar cells. *J. Mater. Chem. A* **2019**, *7*, 21280–21289. [\[CrossRef\]](#)
14. Kung, P.K.; Li, M.H.; Lin, P.Y.; Chiang, Y.H.; Chan, C.R.; Guo, T.F.; Chen, P.J. A review of inorganic hole transport materials for perovskite solar cells. *Adv. Mater. Interfaces* **2018**, *5*, 1800882. [\[CrossRef\]](#)
15. Yang, S.; Zhang, Z.; Chen, H.; Li, C.-Z. Recent advances in perovskite solar cells: Efficiency, stability and lead-free perovskite. *J. Mater. Chem. A* **2017**, *5*, 11462–11482. [\[CrossRef\]](#)
16. Wang, R.T.; Xu, A.F.; Li, W.; Li, Y.; Xu, G. Moisture-Stable FAPbI(3) Perovskite Achieved by Atomic Structure Negotiation. *J. Phys. Chem. Lett.* **2021**, *12*, 5332–5338. [\[CrossRef\]](#) [\[PubMed\]](#)
17. Xu, A.F.; Liu, N.; Xie, F.; Song, T.; Ma, Y.; Zhang, P.; Bai, Y.; Li, Y.; Chen, Q.; Xu, G. Promoting Thermodynamic and Kinetic Stabilities of FA-based Perovskite by an in Situ Bilayer Structure. *Nano Lett.* **2020**, *20*, 3864–3871. [\[CrossRef\]](#) [\[PubMed\]](#)
18. Nair, S.; Gohel, J.V. A study on optoelectronic performance of perovskite solar cell under different stress testing conditions. *Opt. Mater.* **2020**, *109*, 110377. [\[CrossRef\]](#)
19. Juarez-Perez, E.J.; Ono, L.; Maeda, M.; Jiang, Y.; Hawash, Z.; Qi, Y. Photodecomposition and thermal decomposition in methylammonium halide lead perovskites and inferred design principles to increase photovoltaic device stability. *J. Mater. Chem. A* **2018**, *6*, 9604–9612. [\[CrossRef\]](#)
20. Schloemer, T.H.; Raiford, J.A.; Gehan, T.S.; Moot, T.; Nanayakkara, S.; Harvey, S.P.; Bramante, R.C.; Dunfield, S.; Louks, A.E.; Maughan, A.E.; et al. The Molybdenum Oxide Interface Limits the High-Temperature Operational Stability of Unencapsulated Perovskite Solar Cells. *ACS Energy Lett.* **2020**, *5*, 2349–2360. [\[CrossRef\]](#)
21. Tepliakova, M.M.; Mikheeva, A.N.; Somov, P.A.; Statnik, E.S.; Korsunsky, A.M.; Stevenson, K.J. Combination of Metal Oxide and Polytriarylamine: A Design Principle to Improve the Stability of Perovskite Solar Cells. *Energies* **2021**, *14*, 5115. [\[CrossRef\]](#)
22. Tepliakova, M.M.; Mikheeva, A.N.; Frolova, L.A.; Boldyreva, A.G.; Elakshar, A.; Novikov, A.V.; Tsarev, S.A.; Ustinova, M.I.; Yamilova, O.R.; Nasibulin, A.G. Incorporation of vanadium (V) oxide in hybrid hole transport layer enables long-term operational stability of perovskite solar cells. *J. Phys. Chem. Lett.* **2020**, *11*, 5563–5568. [\[CrossRef\]](#) [\[PubMed\]](#)
23. Ma, H.; Yuan, L.; Chen, Q.; Fu, J.; Zhang, J.; Jiang, Z.; Dong, B.; Zhou, Y.; Yin, S.; Song, B. Conjugated copolymers as doping- and annealing-free hole transport materials for highly stable and efficient p-i-n perovskite solar cells. *J. Mater. Chem. A* **2021**, *9*, 2269–2275. [\[CrossRef\]](#)
24. Kim, G.-W.; Kang, G.; Kim, J.; Lee, G.-Y.; Kim, H.I.; Pyeon, L.; Lee, J.; Park, T. Dopant-free polymeric hole transport materials for highly efficient and stable perovskite solar cells. *Energy Environ. Sci.* **2016**, *9*, 2326–2333. [\[CrossRef\]](#)
25. Hummelen, J.C.; Knight, B.J.; LePeq, F.; Wudl, F.; Yao, J.; Wilkins, C.L.J.J.o.O.C. Preparation and Characterization of Fulleroid and Methanofullerene Derivatives. *J. Org. Chem.* **1995**, *60*, 532–538. [\[CrossRef\]](#)
26. Tepliakova, M.M.; Akkuratov, A.V.; Tsarev, S.A.; Troshin, P.A. Suzuki polycondensation for the synthesis of polytriarylamines: A method to improve hole-transport material performance in perovskite solar cells. *Tetrahedron Lett.* **2020**, *61*, 152317. [\[CrossRef\]](#)
27. Mikheeva, A.; Kuznetsov, I.; Tepliakova, M.; Elakshar, A.; Gapanovich, M.; Gladush, Y.; Perepelitsina, E.; Sideltsev, M.; Akhiamova, A.; Piryazev, A.; et al. Novel Push-Pull Benzodithiophene-Containing Polymers as Hole-Transport Materials for Efficient Perovskite Solar Cells. *Molecules* **2022**, *27*, 8333. [\[CrossRef\]](#)
28. Mišićák, R.; Novota, M.; Weis, M.; Cigán, M.; Šiffalovič, P.; Nádaždy, P.; Kožíšek, J.; Kožíšková, J.; Pavúk, M.; Putala, M. Effect of alkyl side chains on properties and organic transistor performance of 2,6-bis(2,2'-bithiophen-5-yl)naphthalene. *Synth. Met.* **2017**, *233*, 1–14. [\[CrossRef\]](#)
29. Iovu, M.C.; Sheina, E.E.; Gil, R.R.; McCullough, R.D. Experimental Evidence for the Quasi-Living: Nature of the Grignard Metathesis Method for the Synthesis of Regioregular Poly(3-alkylthiophenes). *Macromolecules* **2005**, *38*, 8649–8656. [\[CrossRef\]](#)
30. King, S.; Sommer, M.; Huettner, S.; Thelakkat, M.; Haque, S.A. Charge separation and recombination in self-organizing nanostructured donor-acceptor block copolymer films. *J. Mater. Chem.* **2009**, *19*, 5436–5441. [\[CrossRef\]](#)
31. Sanehira, E.; Tremolet de Villers, B.; Schulz, P.; Reese, M.; Ferrere, S.; Zhu, K.; Lin, L.; Berry, J.; Luther, J. The Influence of Electrode Interfaces on the Stability of Perovskite Solar Cells: Reduced Degradation using MoOx/Al for Hole Collection. *ACS Energy Lett.* **2016**, *1*, 38–45. [\[CrossRef\]](#)
32. Khenkin, M.V.; Katz, E.A.; Abate, A.; Bardizza, G.; Berry, J.J.; Brabec, C.; Brunetti, F.; Bulović, V.; Burlingame, Q.; Di Carlo, A.; et al. Consensus statement for stability assessment and reporting for perovskite photovoltaics based on ISOS procedures. *Nat. Energy* **2020**, *5*, 35–49. [\[CrossRef\]](#)

Disclaimer/Publisher's Note: The statements, opinions and data contained in all publications are solely those of the individual author(s) and contributor(s) and not of MDPI and/or the editor(s). MDPI and/or the editor(s) disclaim responsibility for any injury to people or property resulting from any ideas, methods, instructions or products referred to in the content.